Hindawi
International Journal of Antennas and Propagation
Volume 2023, Article ID 5515263, 9 pages
https://doi.org/10.1155/2023/5515263

Research Article

Ultra-Wideband Fractal Ring Antenna for Biomedical Applications

Ilyas Saleem ,[1] Umair Rafique ,[2] Shobit Agarwal,[3] Hüseyin Şerif SAVCI ,[4] Syed Muzahir Abbas ,[1] and Subhas Mukhopadhyay[1]

[1]*Faculty of Science and Engineering, School of Engineering, Macquarie University, Sydney, NSW 2109, Australia*
[2]*Center for Wireless Communications, Faculty of Information Technology and Electrical Engineering, University of Oulu, 90570 Oulu, Finland*
[3]*Department of Electrical, Electronic and Information Technology, Università di Bologna, Bologna Campus, Bologna, Italy*
[4]*Electrical and Electronics Engineering Department, College of Engineering and Natural Sciences, Istanbul Medipol University, Istanbul 34810, Turkey*

Correspondence should be addressed to Ilyas Saleem; ilyas.saleem@students.mq.edu.au and Syed Muzahir Abbas; syed.abbas@mq.edu.au

Received 12 July 2023; Revised 3 September 2023; Accepted 8 September 2023; Published 28 September 2023

Academic Editor: Muhammad Zubair

In this paper, an efficient, coplanar waveguide (CPW)-fed printed circular ring fractal ultra-wideband (UWB) antenna is presented for biomedical applications. In UWB technology, short-range wireless communication is possible with low transceiving power, a characteristic that is particularly advantageous in the context of microwave and millimeter-wave (mmWave) medical imaging. In the proposed antenna configuration, the UWB response is achieved by introducing wedged slots in the radiating patch, designed on a low-loss substrate. A CPW partial ground plane is truncated from the edges to optimize the antenna impedance. Experimental results indicate the antenna's robust performance across the frequency range of 3.2–20 GHz. The well-matched measured and simulated results confirm our contribution's employability. Furthermore, a time-domain study offers valuable insights into how the antenna responds to transient signals, highlighting its responsiveness and adaptability to biomedical applications.

1. Introduction

Biomedical applications such as stents, implants, and dental and surgical fixtures need biocompatibility and exceptional mechanical characteristics [1–4]. Therapeutic and diagnostic instruments for medical checkups, i.e., electroencephalogram (EEG), magnetic resonance imaging (MRI), and ultrasonic devices, use transducers [5, 6]. In microwave and millimeter-wave (mmWave) medical and monitoring applications, ultra-wideband (UWB) technology is preferred because of its higher transmission rate, reliability, multipath component resolution, and easy penetration [7–13]. UWB is a recognized technology that uses multiplexing, beamforming, and diversity together to improve the performance of a wireless system in the presence of fading and interference [14–18]. Moreover, UWB has low output power, which satisfies the safety concerns of regulatory authorities for continuous on-body operation since low-energy signals with less electromagnetic sensitivity can neither affect human tissues nor obstruct other medical signals [19–22]. Therefore, in this day and age, UWB technology is being commonly used in biomedical applications that have transducers, and an ingenious UWB antenna turns out to be a vital component for reliable medical imaging and clinical equipment as it provides extra liberty to designers to choose from a wider frequency range [13, 23–28].

Designing a printed antenna with decent radiation performance is simple, but tailoring a design suitable for multiple frequencies and pattern selectivity is not easy. To address this, several UWB antennas with a significant gain over wide frequency bands [29–31] have been recently designed. While these antennas perform effectively within the UWB frequency range and have high gains, their size renders them unsuitable for practical use. For biomedical applications, especially multisensor imaging gadgets, an antenna needs to be compact because a small unit antenna cell allows the placement of multiple antenna elements in an array configuration, eventually increasing imaging resolution. For this purpose, the researchers have realized compactness by increasing the relative permittivity (ϵ_r) of the substrate, adding repetitive structure, and introducing slots [32, 33]. Such strategies ensured compactness at the cost of low directivity and impedance matching. In short, for biomedical applications, an antenna should be small, have high directivity and a wide bandwidth, and enable high penetration inside the human body.

In this work, a low-profile UWB antenna is proposed for biomedical applications. The miniaturization is achieved by designing fractal geometry, and to simplify the fabrication process, a ground plane is placed on the same side as the radiating patch that corresponds to the coplanar waveguide (CPW) technique. For improved impedance matching, the corners of the ground plane are truncated. The presented configuration achieves a wide impedance bandwidth of 16.8 GHz, ranging from 3.2 to 20 GHz. Furthermore, the antenna maintains consistent behavior in terms of both radiation and input impedance across the entire operating range. This feature makes it suitable for both near- and far-field microwave and mmWave medical imaging.

Table 1 offers a comprehensive comparative analysis of various UWB antennas designed for biomedical applications. The comparison encompasses factors such as dimensions, dielectric material, ϵ_r, operating frequency, fractional bandwidth (FBW), and gain. Upon closer examination, it becomes evident that the proposed antenna design showcases a wide frequency bandwidth of 16.8 GHz, indicating its adaptability for diverse applications across the UWB spectrum. Furthermore, a substantial gain of 5.36 dBi and FBW of 144.82% further emphasize the effectiveness of the proposed design in signal reception and transmission, making it a promising choice for biomedical applications where efficient and reliable signal transmission is paramount.

The rest of the organization of this manuscript is as follows: Section 2 explains the antenna design process and its optimization strategy, along with the results. Section 3 contains details of the fabrication and experimental setup, supplemented by an insightful comparison between the simulated and measured results. Section 4 presents the time-domain analysis and group delay response both in side-by-side and face-to-face configurations. Finally, concluding remarks are mentioned in Section 5.

2. Fractal Antenna Design

Figure 1 shows the geometry of the anticipated UWB antenna with an overall size of 25×35 mm^2, while the rest of the antenna parameters are listed in Table 2. The substrate used for the antenna design is RT/Duroid 5880 with ϵ_r of 2.2 and a height (h) of 0.787 mm. From Figure 1, it can be seen that the circular radiating patch consists of 12 wedged slots. The slots are designed by combining a circular element having a diameter (D) and a thin strip having length and width denoted by L_1 and W_1, as shown in Figure 1. This approach led to the realization of fractal geometry. For improved impedance matching in the UWB frequency band, a modified CPW feed technique is utilized. A modification in the ground plane is carried out by meandering the edges in a curved shape, as depicted in Figure 1. With the current gap between W_F and W_G set at 0.2 mm, it is crucial to highlight that modifying this parameter emerges as a notable technique for achieving the desired frequency response, primarily attributed to the coupling effect.

The design process of the proposed antenna starts with the configuration of a conventional CPW-fed circular monopole antenna (see Figure 2a), and its respective reflection coefficient (S_{11}) is plotted in Figure 3. It can be observed that the design of Figure 2(a) is operating well in the frequency range of 3-4 GHz and 10–30 GHz. To get resonance in the UWB range and to improve impedance matching, 12 wedge slots are etched into the circular patch, as shown in Figure 2(b). The introduction of slots tends to achieve UWB response from 3.2 to 25 GHz (see Figure 3). Further improvement in impedance matching is carried out by meandering the edges of the ground plane, as shown in Figure 2(c), while corresponding S_{11} is shown in Figure 3. CST Microwave Studio v2022 is used for the design and simulation processes.

3. Fabrication and Measurement

For the verification of simulated data, a prototype of the proposed antenna is fabricated using the LPKF machine, as shown in Figure 4. The fabricated prototype is then tested using a Rohde & Schwarz (R&S) vector network analyzer (VNA) to measure its actual performance.

A comparison between the simulated and measured S_{11} characteristics of the proposed antenna is shown in Figure 5. Due to measurement equipment limitations, the S_{11} characteristics are measured up to 20 GHz. It can be noticed that the antenna is operating well in the frequency range of 3.2–20 GHz and offers an impedance bandwidth of 16.8 GHz. It is also noticeable from Figure 5 that the trends of the simulated and measured curves are similar, yet the values of the measured data are slightly shifted to the left when compared with the simulated ones. There are two main reasons for this: (i) human error in in-house fabrication and (ii) the use of conductive silver epoxy adhesive for soldering coaxial connectors to the transmission line (simulation does not consider variations from soldering).

Figure 6 depicts the simulated and measured two-dimensional (2D) radiation patterns for yz- and xz-planes. The radiation characteristics were computed for the 4, 8, 12, and 16 GHz frequency bands. As shown in Figure 6, the antenna has bidirectional properties for the yz-plane and omnidirectional properties for the xz-plane. In addition, excellent coverage is evident since the offered antenna displays almost constant response over the operating bandwidth.

Table 1: Comparative analysis among previously presented and proposed UWB antennas meant for biomedical applications.

Ref.	Dimensions (mm^2)	Dimensions (λ^2)	Dielectric material	ε_r	Frequency band (GHz)	FBW (%)	Peak gain (dBi)
[34]	14.9 × 33.14	0.34 × 0.77	FR-4	4.4	3–11	114.28	4.74
[35]	50 × 60	2.9 × 3.5	Denim substrate	1.4	7-28	120	10.1
[36]	31 × 31	0.72 × 0.72	RT/Duroid 5870	2.33	3.04–11	113.39	7.5
[37]	16 × 21	0.42 × 0.55	FR-4	4.4	3.4–12.5	114.5	5.16
[38]	23.1 × 32	0.58 × 0.8	FR-4	4.6	3.1–12	117.88	3.54
[39]	29 × 27	0.87 × 0.81	FR-4	4.4	3–15	133.33	—
[40]	51 × 95	0.93 × 1.74	FR-4	4.4	1–10	163.63	—
[41]	20 × 28 16 × 22	0.49 × 0.69 0.39 × 0.54	FR-4	4.4	2.95–12	121	4 3.6
Proposed	25 × 35	0.96 × 1.35	RT/Duroid 5880	2.2	3.2–20	144.82	5.36

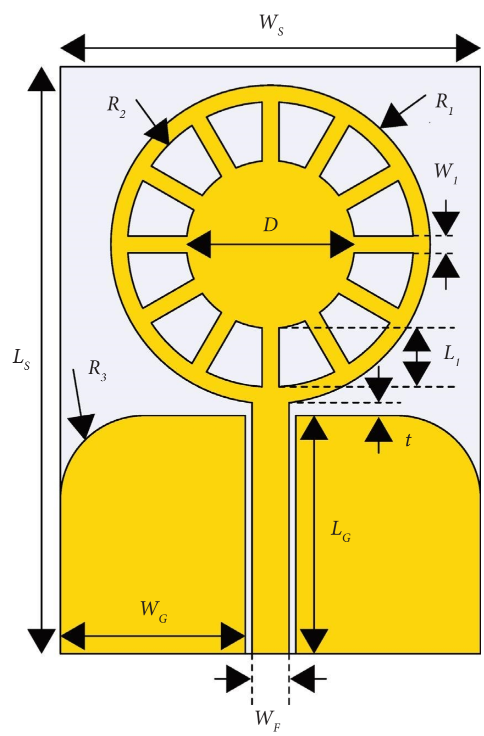

Figure 1: Geometry of the proposed antenna.

Table 2: Optimal design parameters of the proposed antenna (all dimensions in mm).

Parameter	W_S	L_S	W_F	W_G	L_G	t
Value	25	35	2.4	11	14.2	0.8
Parameter	R_1	R_2	R_3	D	W_1	L_1
Value	9.5	8.5	5	10	1	3.5

Figure 7 shows the surface current distribution of the proposed antenna at different frequencies. It is observed that the transmission line is perfectly matched at 50Ω with fewer losses, and all current is reaching the radiating element. At lower frequencies, current distribution is concentrated around the transmission line and lower half of the radiating patch, as shown in Figures 7(a) and 7(b), whereas at higher frequencies, the current dissipates almost equally, creating an electrical loop (see Figures 7(c) and 7(d)).

Figure 8(a) illustrates the realized gain of the proposed antenna as a function of frequency. It can be noted that the gain is increasing with the increase in frequency. From simulations, the minimum and maximum gain values are noted to be 1.52 dBi and 5.36 dBi at 3.2 GHz and 20 GHz, respectively. The measured minimum gain value is noted to be 1 dBi at 3.2 GHz, and the maximum value is observed to be ≈ 4.4 dBi at 16 GHz. Here, it is essential to mention that the gain is measured only up to 16 GHz, constrained by the

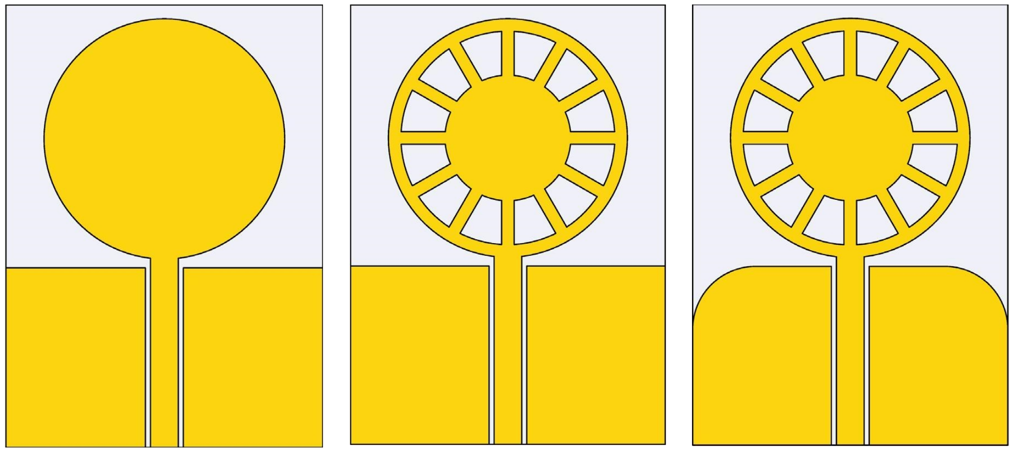

FIGURE 2: Design evolution of the proposed antenna (a) Step-1 (b) Step-2 (c) Step-3 (proposed).

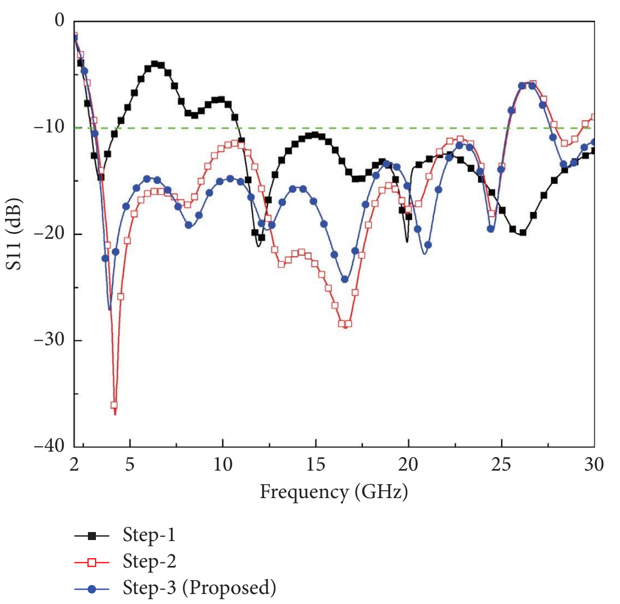

FIGURE 3: Comparison of S_{11} characteristics of antenna designs shown in Figure 2.

measurement setup. The proposed antenna's radiation and total efficiency results are shown in Figure 8(b). As observed, the radiation and total efficiencies are $>85\%$ for the entire operating range.

4. Time-Domain Analysis

It is vital to evaluate the antenna's performance in the time domain for near-field microwave medical imaging applications [13, 42]. Consequently, two identical antennas are positioned in a side-by-side and face-to-face configuration, maintaining a 30 cm separation between them. This arrangement is depicted in Figures 9(a) and 9(b), with both antennas operating in a transceiver mode.

To evaluate the time-domain performance of the proposed antenna, a Gaussian pulse with an operating range of 1–20 GHz is used to excite antennas. The normalized

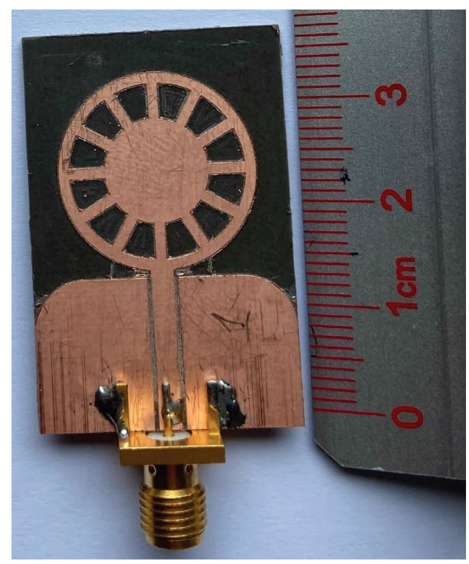

FIGURE 4: Fabricated prototype of the proposed antenna.

amplitudes of the input and output signals for both setups are shown in Figures 10(a) and 10(b). The cross-correlation between transmitted and received pulses is calculated using the below equation, known as the fidelity factor (FF) [43]:

$$\mathrm{FF} = \max\left[\frac{\int_{-\infty}^{\infty} S_t(t) S_r(t+\tau)\mathrm{d}\tau}{\sqrt{\int_{-\infty}^{\infty} |S_t(t)|^2 \mathrm{d}t \int_{-\infty}^{\infty} |S_r(t)|^2 \mathrm{d}t}}\right], \quad (1)$$

where $S_t(t)$ corresponds to the transmitted signal, $S_r(t)$ represents the received signal, and the group delay is denoted by τ. The FF values for both side-by-side and face-to-face configurations are listed in Table 3. In a face-to-face configuration, the FF value is high, which shows less distortion in the transmitted signal.

For UWB antennas, minimal distortion over the entire UWB range is desired. To find the dispersion characteristics and phase distortion of an antenna, the average delay between the center of the transient output and the input signal is measured; this phenomenon is known as group delay.

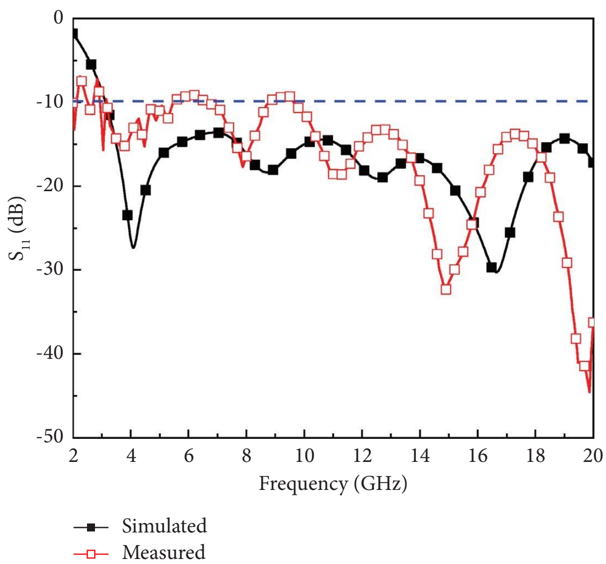

FIGURE 5: S_{11} characteristics of the proposed UWB antenna.

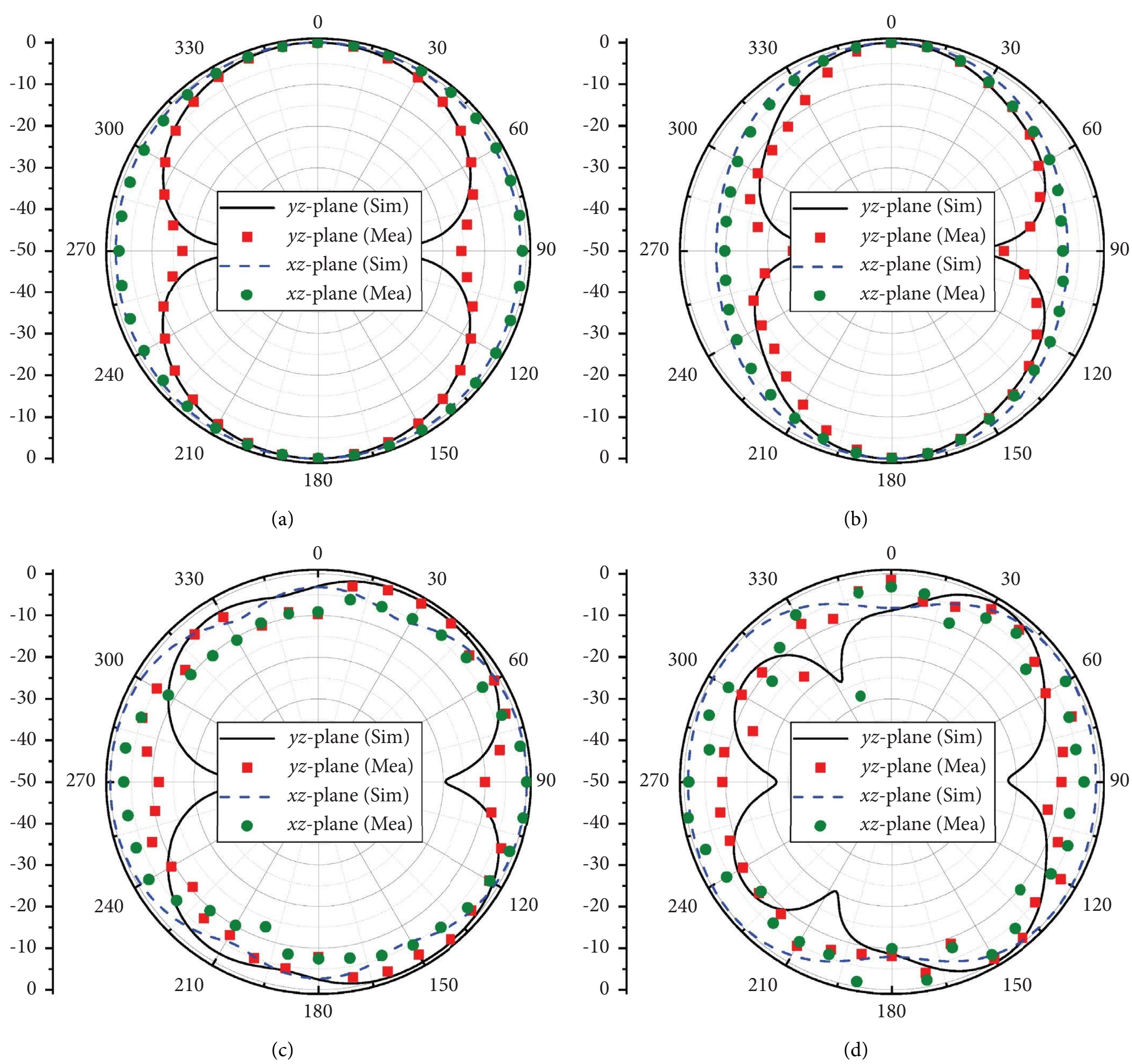

FIGURE 6: Radiation patterns of the proposed antenna at (a) 4 GHz, (b) 8 GHz, (c) 12 GHz, and (d) 16 GHz.

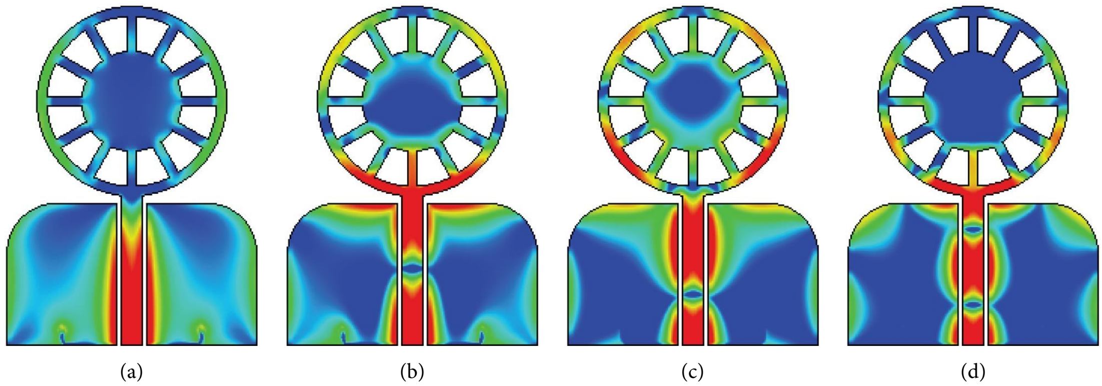

Figure 7: Simulated surface current distribution of the proposed antenna at (a) 4 GHz, (b) 8 GHz, (c) 12 GHz, and (d) 16 GHz.

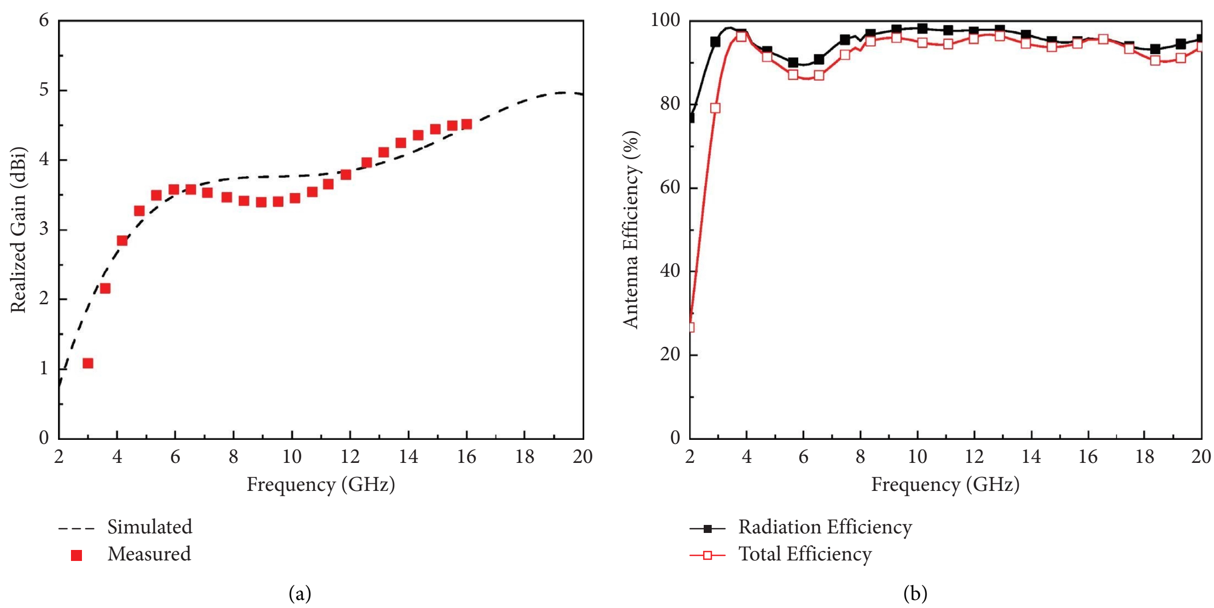

Figure 8: (a) Realized gain and (b) efficiency of the proposed antenna.

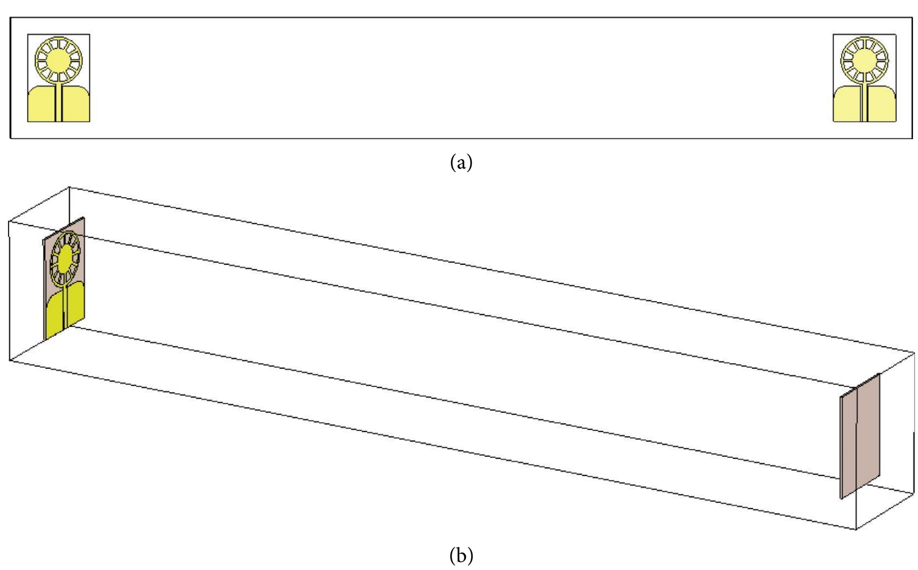

Figure 9: Time-domain analysis configurations: (a) side-by-side; (b) face-to-face.

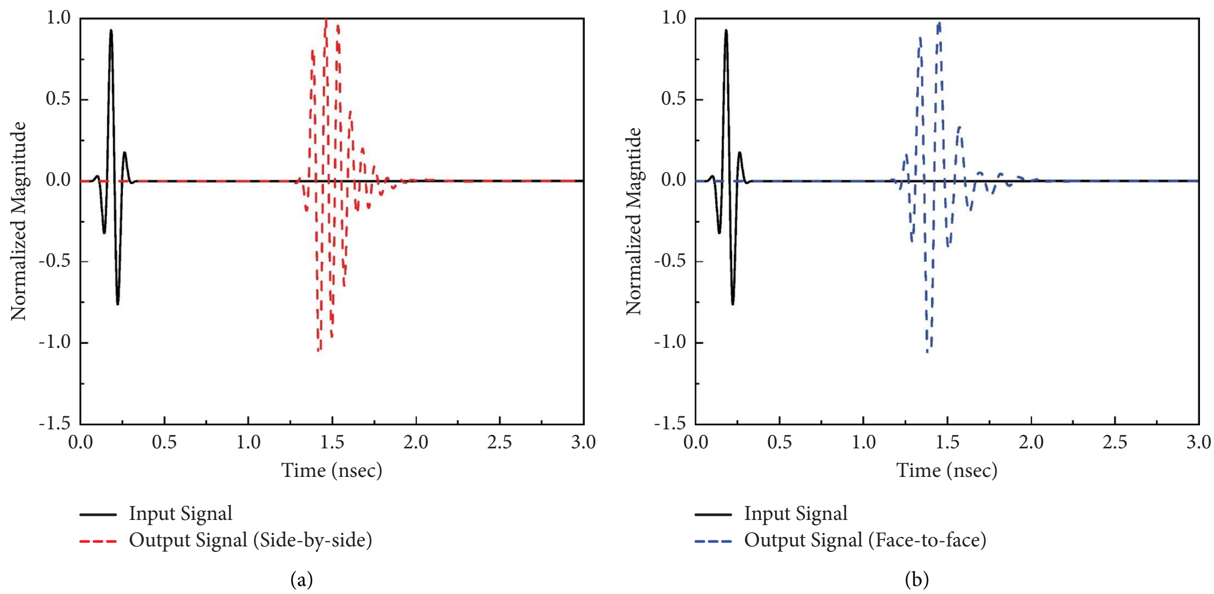

Figure 10: Input and output signals for (a) side-by-side and (b) face-to-face configurations.

Table 3: Fidelity factor of the proposed antenna.

Side-by-side (%)	Face-to-face (%)
76.86	80

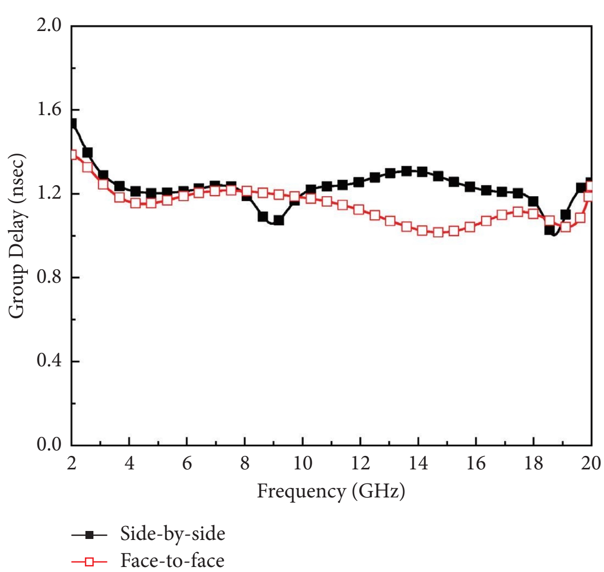

Figure 11: Group delay response of the proposed antenna.

Figure 11 demonstrates that both side-by-side and face-to-face configurations have a peak value of 1.37 ns, indicating that less distortion will occur during the transmission of short pulses.

5. Conclusion

A fractal UWB planar antenna is designed and presented for biomedical applications. The radiating element is composed of a modified CPW-fed circular ring fractal structure. To improve impedance matching, the corners of the ground plane are modified with meandering arcs. The planar fractal antenna exhibits an impedance and FBW of 16.8 GHz and 144.82%, respectively, ranging from 3.2 to 20 GHz. Moreover, the designed antenna showcases nearly constant radiation characteristics across its operational bandwidth. The time-domain performance of the antenna is also evaluated, and acceptable characteristics suitable for a range of biomedical applications, especially microwave and mmWave medical imaging, are observed.

Data Availability

The data used to support the findings of this study are included within the article.

Conflicts of Interest

The authors declare that they have no conflicts of interest.

Acknowledgments

The study was funded by the Macquarie University Research Excellence Scholarship (MQRES) and the Australian Government's Research Training Pathway (RTP) Scholarship. Open access publishing was facilitated by Macquarie University, as part of the Wiley-Macquarie University agreement via the Council of Australian University Librarians.

References

[1] G. Shin, W. Kim, M. C. Kim et al., "A deionized water-infilled dual-layer insulator-applied brain-implanted UWB antenna for wireless biotelemetry applications," *IEEE Transactions on Antennas and Propagation*, vol. 70, no. 8, pp. 6469–6478, 2022.

[2] F. Faisal, M. Zada, H. Yoo, I. B. Mabrouk, M. Chaker, and T. Djerafi, "An ultra-miniaturized antenna with ultra-wide bandwidth for future cardiac leadless pacemaker," *IEEE*

Transactions on Antennas and Propagation, vol. 70, no. 7, pp. 5923–5928, 2022.

[3] M. Frank, F. Lurz, M. Kempf, J. Röber, R. Weigel, and A. Koelpin, "Miniaturized ultra-wideband antenna design for human implants," in *Proceedings of the 2020 IEEE Radio and Wireless Symposium (RWS)*, pp. 48–51, San Antonio, TX, USA, January 2020.

[4] Z. Bao, Y.-X. Guo, and R. Mittra, "An ultrawideband conformal capsule antenna with stable impedance matching," *IEEE Transactions on Antennas and Propagation*, vol. 65, no. 10, pp. 5086–5094, 2017.

[5] M. Wang, L. Crocco, and M. Cavagnaro, "Antipodal vivaldi antenna with ceramic cone lens for biomedical microwave imaging systems," in *Proceedings of the 2021 15th European Conference on Antennas and Propagation (EuCAP)*, pp. 1–5, Dusseldorf, Germany, March 2021.

[6] A. Alemaryeen, S. Noghanian, and R. Fazel-Rezai, "Antenna effects on respiratory rate measurement using a UWB radar system," *IEEE Journal of Electromagnetics, RF and Microwaves in Medicine and Biology*, vol. 2, no. 2, pp. 87–93, 2018.

[7] S. Rashid, L. Jofre, A. Garrido et al., "3-D printed UWB microwave bodyscope for biomedical measurements," *IEEE Antennas and Wireless Propagation Letters*, vol. 18, no. 4, pp. 626–630, 2019.

[8] J. Shang and Y. Yu, "An ultrawideband capsule antenna for biomedical applications," *IEEE Antennas and Wireless Propagation Letters*, vol. 18, no. 12, pp. 2548–2551, 2019.

[9] A. Arayeshnia, A. Madannejad, J. Ebrahimizadeh, F. Ravanbakhsh, M. D. Perez, and R. Augustine, "Miniaturized CPW-fed bowtie slot antenna for wearable biomedical applications," in *Proceedings of the 2020 14th European Conference on Antennas and Propagation (EuCAP)*, pp. 1–4, Copenhagen, Denmark, March 2020.

[10] A. Abohmra, J. ur Rehman Kazim, M. A. Imran et al., "Ultra-wideband hybrid PICA terahertz antenna for high-resolution biomedical imaging," in *Proceedings of the 2020 IEEE International Symposium on Antennas and Propagation and North American Radio Science Meeting*, pp. 1759-1760, Montreal, QC, Canada, July 2020.

[11] X. Lin, Y. Chen, Z. Gong, B.-C. Seet, L. Huang, and Y. Lu, "Ultrawideband textile antenna for wearable microwave medical imaging applications," *IEEE Transactions on Antennas and Propagation*, vol. 68, no. 6, pp. 4238–4249, 2020.

[12] M. Mirzaee, A. Mirbeik-Sabzevari, and N. Tavassolian, "10 GHz-100 GHz compact double-ridge horn antenna for ultra-wideband millimeter-wave biomedical imaging applications," in *Proceedings of the 2020 IEEE International Symposium on Antennas and Propagation and North American Radio Science Meeting*, pp. 1421-1422, Montreal, QC, Canada, July 2020.

[13] U. Rafique, S. Pisa, R. Cicchetti, O. Testa, and M. Cavagnaro, "Ultra-wideband antennas for biomedical imaging applications: a survey," *Sensors*, vol. 22, no. 9, p. 3230, 2022.

[14] N. O. Parchin, H. J. Basherlou, Y. I. A. Al-Yasir, A. A. S. Alabdullah, and R. A. Abd-Alhameed, "Ultra-wideband MIMO diversity antenna system for future handsets," in *Proceedings of the 2020 14th European Conference on Antennas and Propagation (EuCAP)*, pp. 1–4, Copenhagen, Denmark, March 2020.

[15] Y.-D. Yan, Y.-C. Jiao, and R. Tian, "A novel wideband circular patch antenna with conical radiation pattern," in *Proceedings of the 2019 International Symposium on Antennas and Propagation (ISAP)*, pp. 1–3, Xi'an, China, October 2019.

[16] C. Kissi, M. Särestöniemi, T. Kumpuniemi et al., "Directive low-band UWB antenna for in-body medical communications," *IEEE Access*, vol. 7, pp. 149026–149038, 2019.

[17] Z. Tang, X. Wu, J. Zhan, S. Hu, Z. Xi, and Y. Liu, "Compact UWB-MIMO antenna with high isolation and triple band-notched characteristics," *IEEE Access*, vol. 7, pp. 19856–19865, 2019.

[18] S.-S. You and G.-L. Huang, "Highly efficient ultra-wideband planar folded dipole antenna for mobile applications," in *Proceedings of the 2021 IEEE International Symposium on Antennas and Propagation and USNC-URSI Radio Science Meeting (APS/URSI)*, pp. 735-736, Singapore, December 2021.

[19] A. Maskooki, C. B. Soh, E. Gunawan, and K. S. Low, "Ultra-wideband real-time dynamic channel characterization and system-level modeling for radio links in body area networks," *IEEE Transactions on Microwave Theory and Techniques*, vol. 61, no. 8, pp. 2995–3004, 2013.

[20] M. Särestöniemi, C. Pomalaza-Ráez, C. Kissi, M. Berg, M. Hämäläinen, and J. Iinatti, "WBAN channel characteristics between capsule endoscope and receiving directive UWB on-body antennas," *IEEE Access*, vol. 8, pp. 55953–55968, 2020.

[21] R. Bharadwaj and S. K. Koul, "Experimental analysis of ultra-wideband body-to-body communication channel characterization in an indoor environment," *IEEE Transactions on Antennas and Propagation*, vol. 67, no. 3, pp. 1779–1789, 2019.

[22] S. N. Mahmood, A. J. Ishak, A. Ismail, A. C. Soh, Z. Zakaria, and S. Alani, "ON-OFF body ultra-wideband (UWB) antenna for wireless body area networks (WBAN): a review," *IEEE Access*, vol. 8, pp. 150844–150863, 2020.

[23] M. K. Sharma, M. Kumar, J. P. Saini et al., "Experimental investigation of the breast phantom for tumor detection using ultra-wide band–MIMO antenna sensor (UMAS) probe," *IEEE Sensors Journal*, vol. 20, no. 12, pp. 6745–6752, 2020.

[24] A. Mirbeik-Sabzevari, S. Li, E. Garay, H.-T. Nguyen, H. Wang, and N. Tavassolian, "Synthetic ultra-high-resolution millimeter-wave imaging for skin cancer detection," *IEEE Transactions on Biomedical Engineering*, vol. 66, no. 1, pp. 61–71, 2019.

[25] J. M. Felício, J. R. Costa, and C. A. Fernandes, "Dual-band skin-adhesive repeater antenna for continuous body signals monitoring," *IEEE Journal of Electromagnetics, RF and Microwaves in Medicine and Biology*, vol. 2, no. 1, pp. 25–32, 2018.

[26] J. Wang, M. Leach, E. G. Lim, Z. Wang, R. Pei, and Y. Huang, "An implantable and conformal antenna for wireless capsule endoscopy," *IEEE Antennas and Wireless Propagation Letters*, vol. 17, no. 7, pp. 1153–1157, 2018.

[27] Z. Miao and P. Kosmas, "Multiple-frequency DBIM-TwIST algorithm for microwave breast imaging," *IEEE Transactions on Antennas and Propagation*, vol. 65, no. 5, pp. 2507–2516, 2017.

[28] L. Guo and A. M. Abbosh, "Microwave stepped frequency head imaging using compressive sensing with limited number of frequency steps," *IEEE Antennas and Wireless Propagation Letters*, vol. 14, pp. 1133–1136, 2015.

[29] R. Xu, Z. Shen, and S. S. Gao, "Compact-size ultra-wideband circularly polarized antenna with stable gain and radiation pattern," *IEEE Transactions on Antennas and Propagation*, vol. 70, no. 2, pp. 943–952, 2022.

[30] Y. Chen, Y. He, W. Li, L. Zhang, S.-W. Wong, and A. Boag, "A 3–9 GHz UWB high-gain conformal end-fire Vivaldi antenna array," in *Proceedings of the 2021 IEEE International Symposium on Antennas and Propagation and USNC-URSI Radio*

Science Meeting (APS/URSI), pp. 737-738, Singapore, December 2021.

[31] J. Eichenberger, E. Yetisir, and N. Ghalichechian, “High-gain antipodal vivaldi antenna with pseudoelement and notched tapered slot operating at (2.5 to 57) GHz,” *IEEE Transactions on Antennas and Propagation*, vol. 67, no. 7, pp. 4357–4366, 2019.

[32] X. Y. Liu, Z. T. Wu, Y. Fan, and E. M. Tentzeris, “A miniaturized CSRR loaded wide-beamwidth circularly polarized implantable antenna for subcutaneous real-time glucose monitoring,” *IEEE Antennas and Wireless Propagation Letters*, vol. 16, pp. 577–580, 2017.

[33] H. Zhang, L. Li, C. Liu, Y.-X. Guo, and S. Wu, “Miniaturized implantable antenna integrated with split resonate rings for wireless power transfer and data telemetry,” *Microwave and Optical Technology Letters*, vol. 59, no. 3, pp. 710–714, 2017.

[34] I. M. Danjuma, M. O. Akinsolu, C. H. See, R. A. Abd-Alhameed, and B. Liu, “Design and optimization of a slotted monopole antenna for ultra-wide band body centric imaging applications,” *IEEE Journal of Electromagnetics, RF and Microwaves in Medicine and Biology*, vol. 4, no. 2, pp. 140–147, 2020.

[35] S. N. Mahmood, A. J. Ishak, T. Saeidi et al., “Full ground ultra-wideband wearable textile antenna for breast cancer and wireless body area network applications,” *Micromachines*, vol. 12, no. 3, p. 322, Mar 2021.

[36] M. Z. Mahmud, M. T. Islam, and M. Samsuzzaman, “A high performance UWB antenna design for microwave imaging system,” *Microwave and Optical Technology Letters*, vol. 58, no. 8, pp. 1824–1831, 2016.

[37] M. M. Islam, M. T. Islam, M. Samsuzzaman, and M. R. I. Faruque, “A negative index metamaterial antenna for UWB microwave imaging applications,” *Microwave and Optical Technology Letters*, vol. 57, no. 6, pp. 1352–1361, 2015.

[38] M. M. Islam, M. T. Islam, M. Samsuzzaman, M. R. I. Faruque, and N. Misran, “Microstrip line-fed fractal antenna with a high fidelity factor for UWB imaging applications,” *Microwave and Optical Technology Letters*, vol. 57, no. 11, pp. 2580–2585, 2015.

[39] S. Subramanian, B. Sundarambal, and D. Nirmal, “Investigation on simulation-based specific absorption rate in ultra-wideband antenna for breast cancer detection,” *IEEE Sensors Journal*, vol. 18, no. 24, pp. 10002–10009, 2018.

[40] D. Lee, D. Nowinski, and R. Augustine, “A UWB sensor based on resistively-loaded dipole antenna for skull healing on cranial surgery phantom models,” *Microwave and Optical Technology Letters*, vol. 60, no. 4, pp. 897–905, 2018.

[41] Z. Lasemi and Z. Atlasbaf, “Impact of fidelity factor on breast cancer detection,” *IEEE Antennas and Wireless Propagation Letters*, vol. 19, no. 10, pp. 1649–1653, 2020.

[42] W. Wiesbeck, G. Adamiuk, and C. Sturm, “Basic properties and design principles of UWB antennas,” *Proceedings of the IEEE*, vol. 97, no. 2, pp. 372–385, 2009.

[43] M. A. Khan, U. Rafique, H. Ş. Savci, A. N. Nordin, S. H. Kiani, and S. M. Abbas, “Ultra-wideband pentagonal fractal antenna with stable radiation characteristics for microwave imaging applications,” *Electronics*, vol. 11, no. 13, p. 2061, 2022.